Izvestiya, Atmospheric and Oceanic Physics, Vol. 41, No. 6, 2005, pp. 713–725. Translated from Izvestiya AN. Fizika Atmosfery i Okeana, Vol. 41, No. 6, 2005, pp. 783–797.

On the Validation of the Poisson Model of Broken Clouds

T. B. Zhuravleva* and A. L. Marshak**

** Institute of Atmospheric Optics, Siberian Division, Russian Academy of Sciences, pr. Akademicheskii 1, Tomsk, 634055 Russia*
e-mail: ztb@iao.ru
*** NASA/GSFC, USA*
e-mail: Alexander.Marshak@nasa.gov
Received January 12, 2004; in final form, December 1, 2004

Abstract—In this study, the validation of a stochastic model of broken clouds based on the Poisson point fluxes is considered. As a prototype of real cloud fields, realizations obtained by the fractionally integrated cascade model are used. To consider variations in the cloud optical thickness (τ) in the Poisson model, additional averaging of radiative characteristics in accordance with the probability density ($f(\tau)$) is proposed. The effective value of the aspect ratio γ, which is the most important input parameter of the Poisson model, is chosen from the condition that the mean nonscattered fluxes calculated with the Poisson and cascade models are consistent. It is shown that, for the conditions of low or moderate cloud fractions ($N < 0.7$) and of moderate light absorption by water droplets (the single scattering albedo $\omega \geq 0.95$), this approach allows a more accurate calculation of the area-average diffuse-solar-radiation fluxes than the independent pixel approximation and than the model of horizontally homogeneous clouds.

INTRODUCTION

Regional climate is influenced by a large number of processes with complicated feedbacks. Among these processes, the interaction between the radiation and cloud fields plays a special role because a variety of types of cloud cover and the high space–time variability of cloud fields significantly influence the dynamics of the radiative regime of the atmosphere–underlying-surface system. In most of the modern models for weather and climate forecasting, calculations of radiative characteristics are based on the two- (or higher) flux approximation of the solution of the one-dimensional deterministic radiative transfer equation (RTE). The assumption on the horizontal homogeneity of clouds leads, in particular, to the phenomenon that the results of numerical simulations agree with satellite measurements only if the radiative codes use the cloud optical-thickness values corresponding to water contents lower than the observed water contents [1]. The difference between calculated and measured radiative characteristics can be decreased by taking into account the spatial inhomogeneity of real cloud fields [2].

In [3], it is shown that important conclusions on the dynamics of the radiative regime in the atmosphere–underlying-surface system can be made from relations between the ensemble-average statistical characteristics of cloud and radiation fields. This understanding promoted the intensive development of the statistical approach to describing radiative transfer in clouds. After the cloud-field model by Mullamaa and his colleagues [4], several stochastic models of one-layer clouds were developed (see, e.g., [5–11]).

The applicability of a stochastic model to calculations of radiative characteristics for subgrid-scale cloud fields is primarily due to the effectiveness and accuracy of the calculation algorithm. At present, the independent pixel approximation (IPA) provides the basis for the most developed method of taking into account the horizontal inhomogeneity of clouds [12, 13]. The essence of this method lies in calculating radiation fluxes by the one-dimensional deterministic RTE and subsequent averaging of the results in accordance with a specified probability density of the cloud optical thickness [14, 15]. It is shown that, for several types of stratiform clouds, such an approach to calculations of area-average solar-radiation fluxes gives satisfactorily accurate results [13, 14, 16–18]. IPA applicability to the calculations of radiative characteristics for clouds of other types is open to question; this remark relates primarily to vertically developed clouds, where optical radiative transfer is determined largely by three-dimensional (3D) effects [19–21].

In the late 1970s, G.A. Titov proposed an approach allowing an effective (in respect to computational burden) and sufficiently accurate consideration for the stochastic geometry of clouds in calculations of the statistical characteristics of solar radiation [6]. In the models intended for weather and climate prediction, the applicability of these algorithms to the parametrization of the radiative characteristics of mesoscale fields of broken clouds depends largely on the results of validation. The validation can be performed on the basis of both the models that have been validated completely or partially by using realistic subgrid-scale fields [22, 23] and complex radiation experiments (see, e.g., [24]). At the

initial stage of validation of Titov's broken cloud model based on Poisson point fluxes, only a small amount of experimental data was available to us. In addition, the available data were not combined; i.e., radiative, optical, and geometrical characteristics of clouds were not always measured simultaneously. Nevertheless, comparisons of simulated statistical characteristics of clouds and radiation with results of the corresponding measurements have shown that the given model describes solar radiative transfer in broken clouds adequately on the whole [6].

This study is aimed at further validation of the statistically homogeneous Poisson model of broken clouds. At this stage of investigation, the data obtained by the fractionally integrated cascade model [25] modified in [26] were taken instead of data on real cloud and radiation fields.

1. STOCHASTIC MODELS OF CLOUDS

1.1. Poisson Model

The one-layer Poisson model of broken clouds is detailed in monograph [6]. Let us briefly summarize the results relating to the statistically homogeneous cloud model (hereafter, the Poisson model) considered in this paper.

The Poisson model is completely determined by the cloud fraction N, cloud geometrical thickness H, and mean horizontal size of clouds D; the input optical characteristics of clouds, namely, the extinction coefficient σ, single scattering albedo ω, and scattering phase function, are taken to be constant for all cloud elements and for all realizations. If the cloud thickness H is fixed, the parameter $\gamma = H/D$ (the aspect ratio), which is more instructive in characterizing the cloud-field geometrical structure, is often used instead of the cloud diameter D.

For statistically homogeneous cloud fields, a closed system of equations is obtained for the mean intensity and effective algorithms are developed for its solution by the Monte Carlo method. The accuracy and applicability range of these equations are estimated through their comparison with the corresponding calculations based on numerical simulations. This comparison have shown that the equations for the mean intensity are sufficiently accurate and can be used to study the effects of random geometry on the radiative properties of broken clouds. The main advantage of the method of closed equations (CEM) is that RTE analytical averaging, performed under certain assumptions on the probabilistic characteristics of the cloud field, allows low-burden calculations of the mean radiative characteristics of clouds.

In [23, 27], the proposed approach is generalized for a multilayer inhomogeneous broken-cloud model with a multitude of input parameters that are bound to contain information on the degree of correlation of clouds lying at different atmospheric levels. The amount of such information is extremely limited; however, the current strong interest in the combined studies of complicated cloud systems gives hope that the necessary data will be available in the coming years.

1.2. Fractionally Integrated Cascade Model

In [25, 28], fractal models are proposed for the spatial distribution of liquid-water in clouds. These models conserve the total water amount within a cloud field. Their advantage lies in the fact that, varying a few easily measurable input parameters, one can obtain different distributions of liquid-water whose spatial correlations correspond to the observed ones. The procedure of constructing some fractal models generated by multiplicative cascades in a overcast sky is described briefly in the Appendix (singular and bounded cascades, fractionally integrated cascade model).

In this study, the horizontal distribution of the liquid-water path (LWP) is simulated using the fractionally integrated cascade model with the power spectrum

$$E(k) \propto k^{-\beta}. \quad (1)$$

In (1), the wave number $k = \pi/r$, the scale r (km), and the LWP probability density correspond to marine stratocumulus clouds [29–31]. The vertical optical thickness of clouds τ is related to the LWP according to the following well-known expression: $\tau = 3LWP/(2\rho r_{\text{eff}})$, where r_{eff} is the effective radius of cloud droplets and ρ is the water density. Therefore, if r_{eff} is fixed, one can switch from the $LWP(x, y)$ distribution to the distribution of optical thickness $\tau_{\min} \le \tau(x, y) \le \tau_{\max}$.

At present, there is no substantiated theory of switching from overcast skys $\tau(x, y)$ to broken clouds $\tau_{\text{bc}}(x, y)$. Therefore, we simulate "holes" in a cloud layer on the basis of the approach proposed in [26]:

$$\tau_{\text{bc}}(x,y) = b\max[\tau(x,y) - a, 0], \quad (2)$$

where $a = \text{const} > 0$ and $b = \text{const} > 0$. The limitation of the optical thickness at a level of $a > \tau_{\min}$ would lead to a decrease in the liquid-water amount in the layer; to avoid such a decrease, we introduce the factor b. Thus, each broken-cloud realization simulated on the basis of the fractionally integrated cascade model (hereafter, the cascade model) is determined by the following parameters:

mean optical thickness $\bar{\tau}$,

parameter p characterizing variations in the optical thickness,

exponent β in (1), and

cloud fraction N related to the parameter a by (2).

In the model version under consideration, it is assumed that the geometrical cloud thickness is constant and the extinction coefficient is independent of height; i.e., $\sigma(z) = \sigma$.

The fractionally integrated cascade model was compared earlier with both additive fractal models (e.g., the

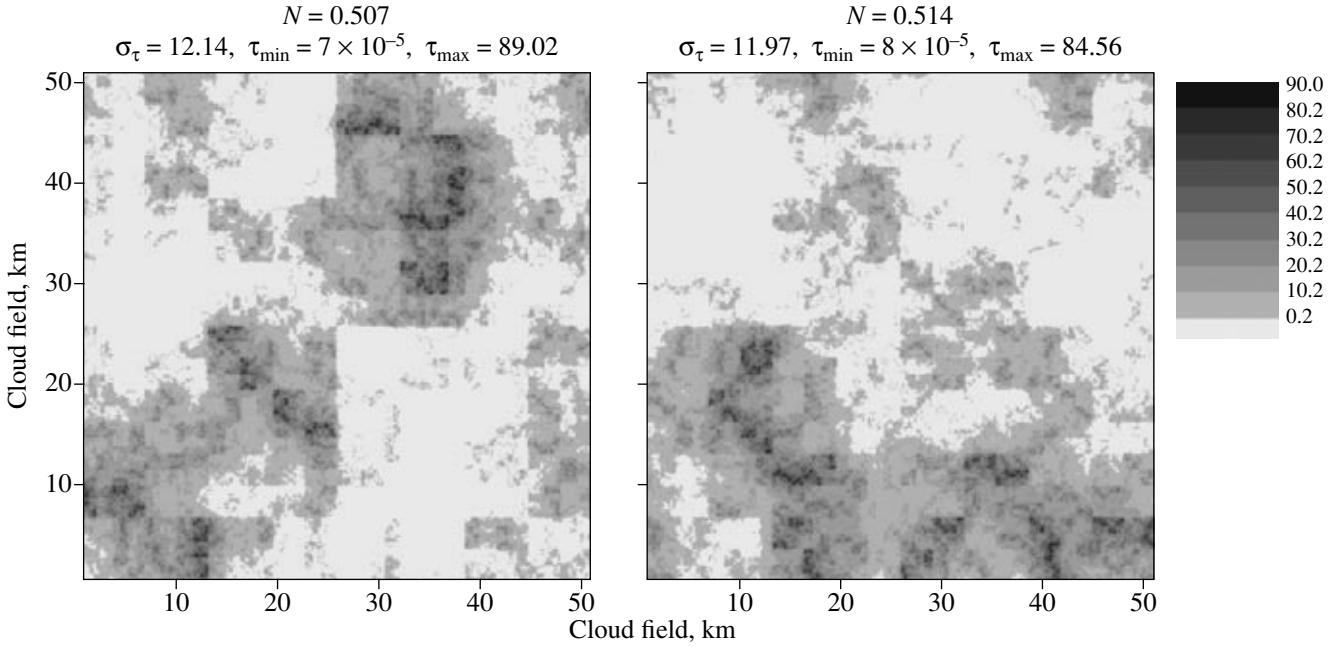

Fig. 1. Examples of realizations of cloud fields in the fractionally integrated cascade model of broken clouds: $a = 11.5$ ($\langle N \rangle = 0.51$) and $\bar{\tau} = 13$.

model of fractional Brownian motion [32]) and multiplicative fractal models (e.g., the model of bounded cascades [33]), which are used for simulation of horizontally inhomogeneous stratocumulus clouds observed from the LANDSAT-type satellites with a high spatial resolution. These comparisons have shown that, among the simplest fractal models, which hold the correlation properties of simulated cloud fields in addition to the mean and standard deviation, the fractionally integrated cascade model provides the most adequate description of fluctuations in the cloud optical thickness.

1.2.1. Statistical characteristics of clouds

As a result of simulation of a multitude of cascade-model realizations for fixed input parameters, we obtain a set of values of the cloud fraction N and distributions of the cloud optical thickness, which change from one realization to another. Several examples of the realizations corresponding to one a value and fixed values of $\bar{\tau}$, p, and β are given in Fig. 1. This figure and the other figures give results corresponding to the values (unless otherwise indicated) $\beta = 5/3$, $p = 0.35$, number of pixels $N_{pix} = 2^9$, pixel size 0.1 km × 0.1 km, and $H = 1$ km.

We will treat the cloud fraction as a random variable characterized by the mean $\langle N \rangle$, standard deviation σ_N, and probability density $f_{cas}(N)$. Hereafter, angular brackets $\langle\rangle$ indicate characteristics averaged over an ensemble of realizations. Numerical experiments showed that simulation of 5000 to 10000 realizations ($M = 5000$–10000) are sufficient for obtainment of reliable statistics. Figure 2 presents the cloud-amount statistical characteristics corresponding to different $\langle N \rangle$ values. Note that as $\langle N \rangle$ increases, the N variability range increases: for example, $(N_{max} - N_{min}) \approx 0.04$ at $\langle N \rangle = 0.1$ and $(N_{max} - N_{min}) \approx 0.08$ at $\langle N \rangle = 0.52$. (N_{max} and N_{min} are the maximum and minimum N values, respectively.)

For a overcast sky, the optical-thickness probability density averaged over a multitude of realizations can be closely approximated by a log-normal distribution (Fig. 3a). For broken clouds, asymmetry is increased as a result of the occurrence of a large number of optically thin clouds (Figs. 3b–3d). This result correlates well with observational data [34]. The minimum and maximum cloud optical thicknesses depend on a realization; hereafter, we use $\langle \tau_{min} \rangle$ and $\langle \tau_{max} \rangle$ values averaged over the multitude of realizations.

Note that the probability density of the optical thickness for real clouds depends on the type of clouds, the underlying surface, the season, etc. For some types of clouds, such as marine stratocumulus and plane cumulus clouds, the probability density of the optical thickness is approximated closely by a Γ-distribution:

$$f_\Gamma(\tau, \nu, \lambda) = \frac{1}{\Gamma(\nu)}(\lambda)^\nu \tau^{\nu-1}\exp(-\lambda\tau), \quad \lambda = \frac{\nu}{\bar{\tau}}, \quad (3)$$

where $\nu = \left(\frac{\bar{\tau}}{\sigma_\tau}\right)^2$ and the standard deviation $\sigma_\tau^2 = \frac{\nu}{\lambda^2}$ [16].

The comparison illustrated by Figs. 3b–3d shows that the probability densities $\langle f_{cas}(N) \rangle$ and $f_\Gamma(\tau)$ are close

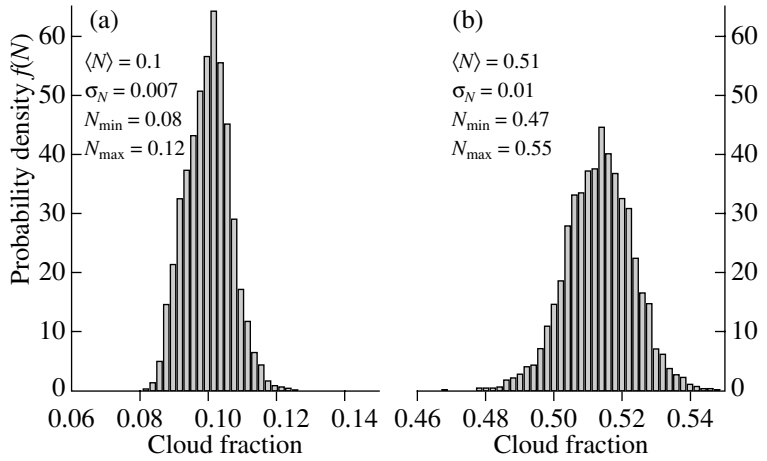

Fig. 2. Statistical characteristics of the cloud fraction in the fractionally integrated cascade model of clouds for different means of N: (a) $a = 21.0$ and (b) $a = 11.5$.

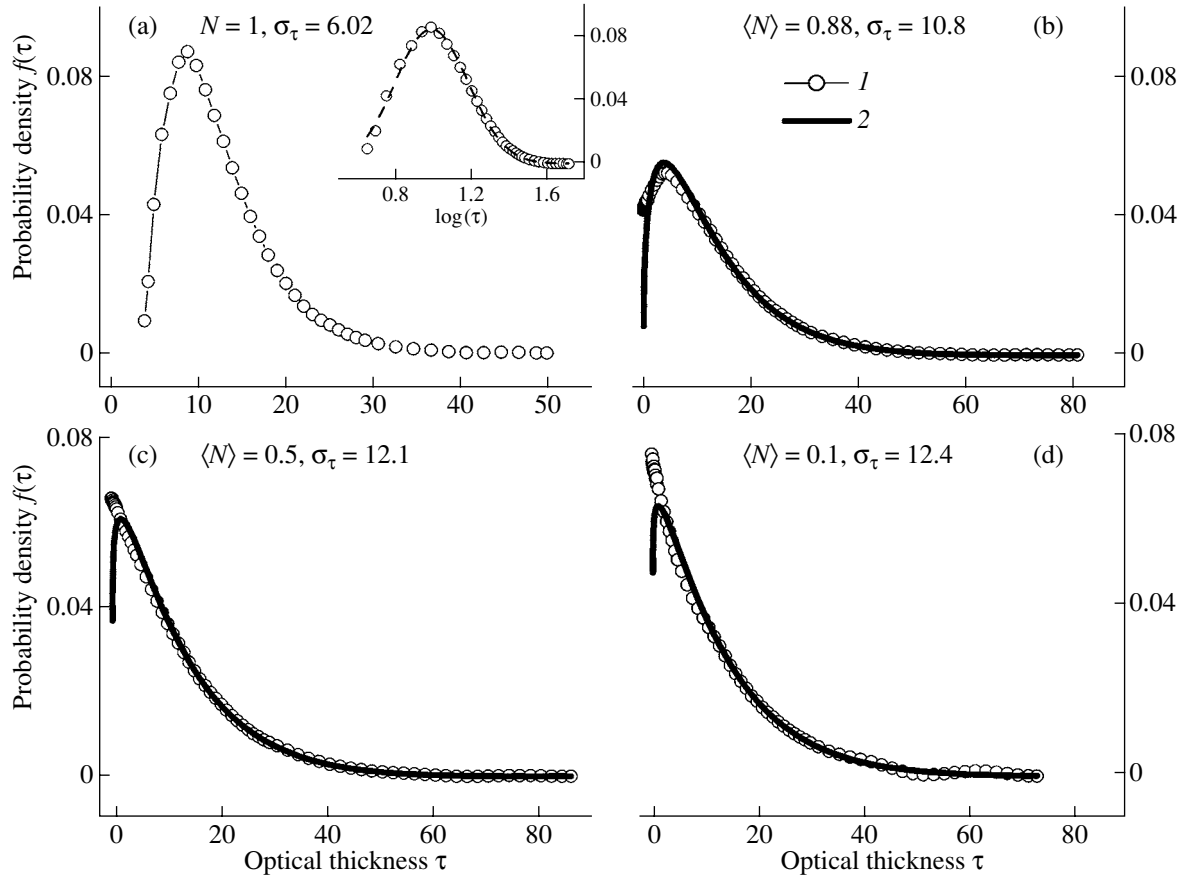

Fig. 3. (*1*) Probability density of the optical thickness in the cascade model of clouds $f_{cas}(\tau)$ and (*2*) the corresponding Γ-distribution $f_\Gamma(\tau)$ for different cloud fractions and $\bar{\tau} = 13$.

in value if $\tau \geq (1.5–2)$. ($f_\Gamma(\tau)$ is calculated at the $\bar{\tau}$ and σ_τ values corresponding to the cascade model.) If the distribution of optical thickness in the cascade model is approximated on the basis of $f_\Gamma(\tau)$, the portion of optically thin clouds is underestimated as $\langle N \rangle$ is decreased. At low and moderate cloud fractions ($\langle N \rangle \leq 0.7$), the function $\langle f_{cas}(N) \rangle$ can be approximated closely by an exponential distribution [34].

1.2.2. Statistical characteristics of radiation

First, we will discuss an efficient procedure of calculating statistical characteristics of radiation (R) averaged over a multitude of realizations in the cascade model. (Hereinafter, the letter R is used to denote the nonscattered S and diffuse Q_s transmissions and albedo A'.)

Taking into account the constructive character of the cascade model, we can calculate the radiative characteristics by using a simple albeit time-consuming procedure. This calculation procedure consists of the consecutive numerical simulation of random cloud-field realizations, "exact" solution of the RTE for each of the realizations, and statistical processing of the ensemble of radiation fields. The solution of the RTE for cloud realizations is time consuming because each cloud realization represents a complicated inhomogeneous three-dimensional medium; therefore, the applicability of the approach considered above is restricted significantly.

To effectively calculate the radiative characteristics averaged over a multitude of cloud realizations, we use the randomization procedure, i.e., introduce an additional randomness [35, 36]. According to this approach, the statistical characteristics of radiation can be obtained on the basis of their random evaluation for m independent photon trajectories chosen randomly in each realization. An optimal number of photon trajectories is chosen on the basis of special numerical tests. Our preliminary calculations have shown that, for the mean-flux calculations, a rather small number of trajectories ($1 \le m \le 1000$ depending on the input parameters of the problem) is sufficient; meanwhile, to calculate the variance, $m \sim 10^4$ should be used.

To simulate radiative characteristics for each of the cloud realizations, the "method of a maximum cross section" is used [37]. The algorithm of calculations of radiation in the three-dimensional inhomogeneous medium, such as a cloud realization of the cascade model, was tested within the framework of the International Project "Intercomparison 3D Radiation Codes" (http://i3rc.gsfc.nasa.gov).

Let a unit solar-radiation flux fall on the upper boundary of the atmosphere in the direction $\mathbf{\Omega}_0 = (\theta_0, \varphi_0)$. ($\theta_0$ and φ_0 are the zenith and azimuth angles, respectively.) At this stage of the study, we assume that the underlying surface is a blackbody (its albedo $A_s = 0$) and neglect the aerosol and molecular constituents of the atmosphere. The calculations are performed using the scattering phase function corresponding to cloud model C1 ($\lambda = 0.69$ μm) [38]. Let us restrict ourselves to the consideration of monochromatic radiation because the transition to the radiative characteristics integrated over the spectrum leads to an increase in the uncertainties caused by inaccuracies in the parametrizations of cloud microphysical characteristics, in the specification of the atmospheric gas model and the spectroscopic information, etc.

The cloud-field areas were equal to (51.2×51.2) km^2. According to the classification of the space–time scales of atmospheric phenomena, such fields correspond to a mesoscale of 20–200 km (a cluster of clouds) [39]. The application of the cascade model to a simulation of the horizontal distribution of liquid-water in large-scale cloud fields is unreasonable because no LWP correlations occur on scales exceeding 50 km [31]. Boundary conditions in horizontal directions were assumed to be periodic.

The stochasticity of radiation fields follows from the stochastic nature of clouds. In [40], by an example of rather small cloud fields (6.4 km × 6.4 km) it was shown that the nonscattered radiation S at the surface in different realizations may vary almost threefold, depending on the parameters of the problem, and the variation coefficient $\nu_S = 100\%\sigma_S/\langle S\rangle$, where σ_S is the standard deviation, can reach 50%. If the cloud field is increased to the sizes considered in this problem (51.2 km × 51.2 km), the variation coefficient $\nu_R = 100\%\sigma_R/\langle R\rangle$ is decreased substantially (Fig. 4). However, in this case, the radiation fluxes calculated by the cascade model are also sufficiently variable, thus necessitating averaging of radiative characteristics over a multitude of realizations.

2. PROCEDURE FOR VALIDATION OF THE BROKEN-CLOUD POISSON MODEL

Before proceeding further, we should find a reasonable way to specify the input parameters for the Poisson model. We were guided by the following two arguments.

First, the CEM proposed by Titov [6] allows an efficient computation of the characteristics averaged over ensembles of cloud realizations $\langle R\rangle_{\text{pois}}$ if the extinction coefficient σ is constant for all cloud elements and for all realizations. Since the mean radiative regimes in clouds of moderate optical thickness ($\tau \ge 5$) change only slightly under small variations in σ (the derivatives of fluxes $\dfrac{\partial Q_s}{\partial \sigma}$ and $\dfrac{\partial A}{\partial \sigma}$ are two or three orders of magnitude smaller than the derivatives of these fluxes with respect to N and D, depending on the parameters), the assumption that σ = const can be considered to be permissible under certain conditions. However, the situation changes significantly when the cloud extinction coefficients are small; namely, the mean fluxes depend significantly on σ and the derivative $\dfrac{\partial Q_s}{\partial \sigma}$ changes its sign at $\sigma \approx 2$–3 km^{-1} ($H = 1$ km) (see Fig. 5). These features should be taken into account because the optical thickness (i.e., the extinction coefficient at a constant geometricalthickness H) of real clouds can vary in a wide range.

To take into account variations in the cloud optical thickness, we average the function $\langle R(\tau, \gamma, N, \theta_0)\rangle_{\text{pois}}$

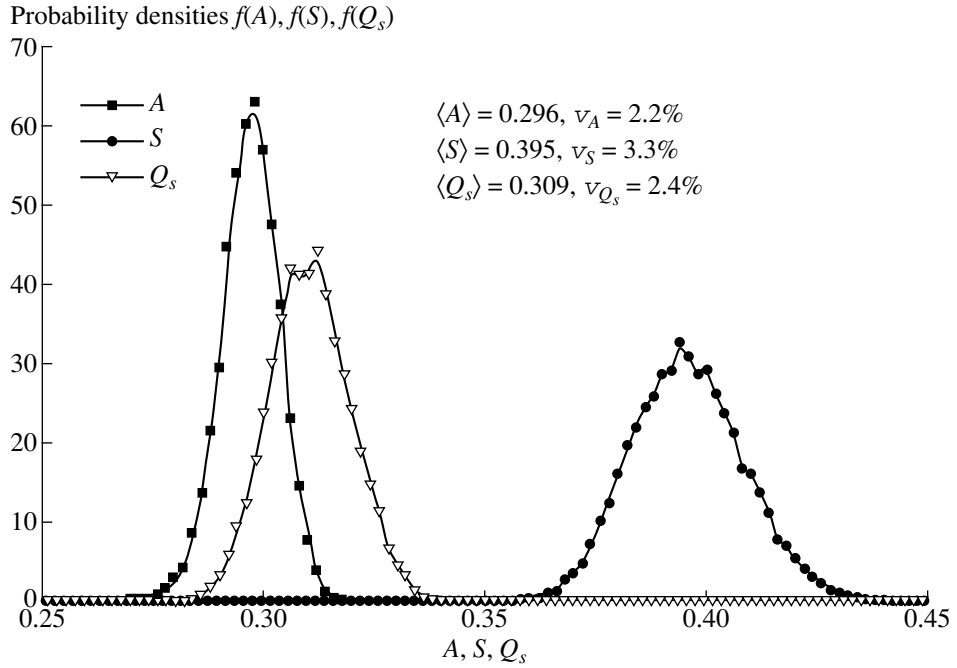

Fig. 4. Statistical characteristics of nonscattered radiation S, diffuse transmission Q_s, and albedo A computed in the fractionally integrated cascade model of clouds: $\langle N\rangle = 0.51$, $\bar{\tau} = 13$, $\sigma_\tau = 12.1$, and $\omega = 1$. The solar zenith angle $\theta_0 = 60°$.

over τ, while assuming that the probability density $f(\tau)$ is known:

$$\rangle R(\gamma, N, \theta_0)\langle_{\text{pois}} = \int_0^\infty \langle R(\tau, \gamma, N, \theta_0)\rangle_{\text{pois}} f(\tau) d\tau, \quad R = S, A, Q_s. \quad (4)$$

The symbol $\rangle R\langle_{\text{pois}}$ denotes the radiative characteristics averaged over the multitude of cloud realizations corresponding to $\tau = \text{const}$ and over the multitude of the possible values of optical thickness. For $f(\tau)$, we use below the function $\langle f_{\text{cas}}(\tau)\rangle$ averaged over the multitude of realizations of the cascade model. According to the results presented in Section 1.2.1, the Γ-distribution written with the parameters corresponding to the $\bar{\tau}$ and σ_τ can be apparently used for averaging (4) if no information on the probability density $f(\tau)$ is available. The estimates of the errors caused by such an approximation require additional studies and are not considered in this paper.

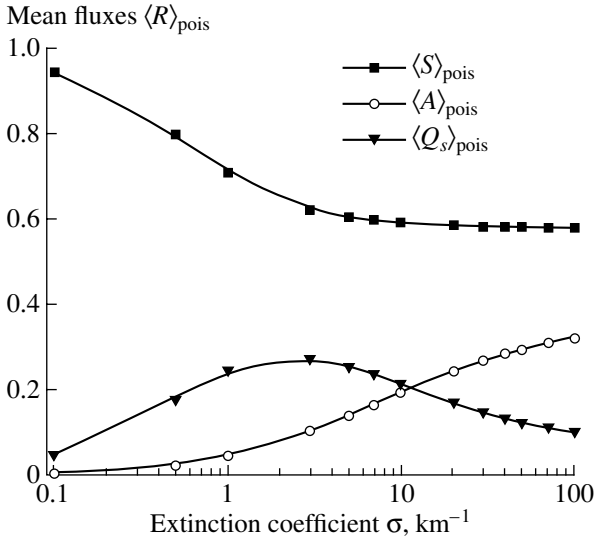

Fig. 5. Effect of the cloud extinction coefficient on the mean radiation fluxes in the Poisson model of broken clouds: $N = 0.3$, $\theta_0 = 60°$, $\gamma = 0.33$, and $\omega = 1$.

Second, the parameter γ is the most important input parameter for the Poisson model. For its specifications, it is necessary to have information on the vertical thickness H and mean horizontal sizes D of clouds. The best but extremely complicated procedure of the combined estimation of the sizes of clouds H and D lies in conducting complex experiments. If the determination of the probability densities for the cloud sizes $f(D)$ and $f(H)$ is problematic for some reason, the cloud geometrical characteristics for other (preferably, similar) regions and atmospheric conditions can be used as a first approximation.

Information from monitoring stations, aircraft, and satellites about the heights of the upper and lower cloud boundaries is generalized and published in a number of papers (see, e.g., [39]). Note that passive satellite measurements (Moderate Resolution Imaging Spectroradiometer, MODIS, and Advanced Very High Resolution Radiometer, AVHRR) determine the upper cloud boundary only. The use of the THOR (Thickness from

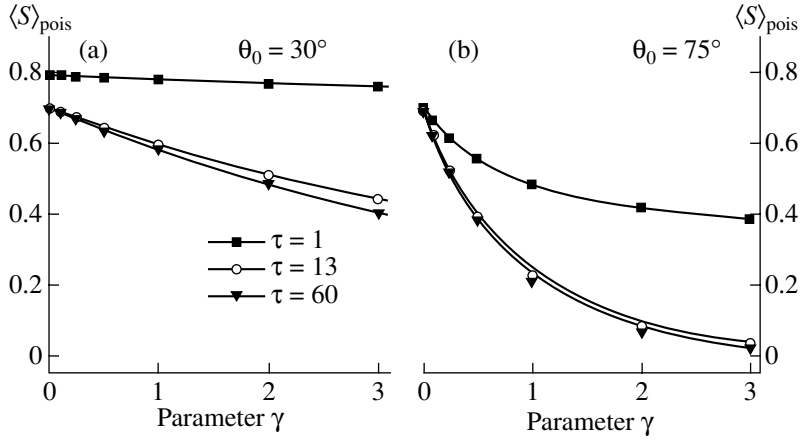

Fig. 6. Mean fluxes of nonscattered radiation $\langle S\rangle_{\text{pois}}$ vs. the parameter γ at different optical thicknesses τ: (a) $\theta_0 = 30°$ and (b) $\theta_0 = 75°$. The cloud fraction $N = 0.3$.

Offbeam Returns) lidar offers prospects for retrieving the cloud geometrical thicknesses [41].

The amount of experimental data on $f(D)$ is rather large [39, 42–44]. It is shown in [45] that the probability density for the horizontal sizes of cumulus clouds over the Florida region decreases exponentially as D increases. According to radiometric measurements performed by the LANDSAT over southern California, the D distribution for twelve types of stratocumulus cloud fields can be approximated by the function $f(D) \sim D^{-\alpha}$, where $1 < \alpha < 3$ [46]. The horizontal sizes of clouds can also be obtained as a result of analysis of the MODIS data [47] and (after launching the CLOUDSAT) of the CLOUDSAT radar data [48].

We emphasize that such a climatological approach to the choice of the parameter γ can initiate errors in the process of Poisson-model validation because data on the vertical and horizontal sizes of clouds vary significantly for different regions, seasons, cloud types, etc.

On the basis of the above remarks, we propose to preset the Poisson model input parameters, taking the cloud fraction N to be equal to $\langle N\rangle$ and choosing the parameter γ such that, at $N = \langle N\rangle$, the mean nonscattered radiation in the Poisson model $\rangle S(\gamma, N, \theta_0)\langle_{\text{pois}}$ is equal to the nonscattered radiation averaged over a multitude of cloud realizations of the cascade model; i.e.,

$$\rangle S(\gamma, N, \theta_0)\langle_{\text{pois}} = \langle S(N, \theta_0)\rangle. \quad (5)$$

The effective value of the parameter γ determined in this manner can differ from its physical value $\gamma = H/D$. The correspondence between these values is of doubtless interest; however, it is not considered in this study.

To conclude this section, we will discuss the mean nonscattered-radiation sensitivity in the Poisson model to γ variations. Calculations show (Fig. 6) that the dependence of $\langle S\rangle_{\text{pois}}$ on γ_0 becomes stronger as the solar zenith angle increases; moreover, even for moderate optical thickness values ($\tau = 13$), the mean nonscattered radiation decreases significantly: $\langle S\rangle_{\text{pois}} \le 0.02$ at $\gamma \ge 3$ ($\theta_0 = 75°$). As the cloud fraction and the cloud optical thickness increase, these regularities begin to reveal themselves at lower θ_0. In addition, we note that, according to [6], the mean scattered-radiation fluxes $\langle A\rangle_{\text{pois}}$ and $\langle Q_s\rangle_{\text{pois}}$ are most sensitive to D variations (i.e., to γ variations at fixed H values) at $N \approx 0.2$–0.5. (According to the experimental data of [45], such cloud-amount values are typical of good-weather cumulus clouds.) This consideration shows that the retrieval of the effective value of γ by (5) is possible for the conditions when the solar zenith angle $\theta_0 \ge 30°$ and the cloud amount $N < 0.7$.

3. RESULTS OF NUMERICAL SIMULATION

Below, we will compare the mean solar-radiation fluxes simulated using the following four cloud models:

(1) The fractionally integrated cascade model, $\langle R\rangle$.

(2) The Poisson model of broken clouds, $\rangle R\langle_{\text{pois}}$:

$$\rangle R(\gamma, N, \theta_0)\langle_{\text{pois}} = \int_{\langle\tau\rangle_{\min}}^{\langle\tau\rangle_{\max}} \langle R(\tau, \gamma, N, \theta_0)\rangle_{\text{pois}}\langle f_{\text{cas}}(\tau)\rangle d\tau. \quad (6)$$

(3) The model of broken clouds under the assumption of horizontally homogeneous (HH) clouds at the mean optical thickness $\bar{\tau}$,

$$R_{\text{HH}} = NR^{\text{cc}}(\bar{\tau}) + (1 - N)R^{\text{cs}}, \quad (7)$$

where the superscripts os and cs relate to the calculations for an overcast sky and a cloudless sky, respectively.

(4) The IPA modified for broken clouds,

$$R_{\text{IPA}} = NR^{\text{cc}}_{\text{IPA}} + (1 - N)R^{\text{cs}}, \quad (8)$$

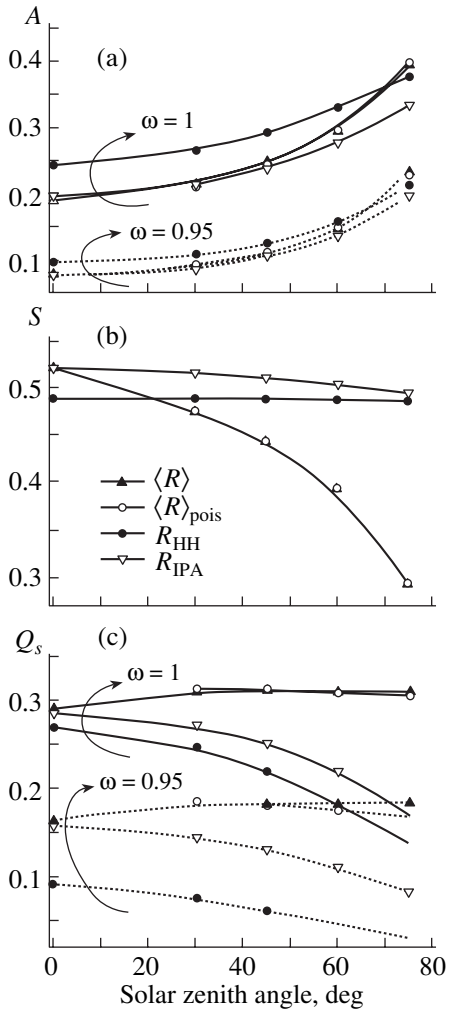

Fig. 7. Radiation fluxes calculated in the IPA and in the cascade, Poisson, and HH models of clouds at $\langle N\rangle = 0.51$, $\bar{\tau} = 13$, and $\sigma_\tau = 12.1$.

where

$$R^{cc}_{IPA} = \int_{\langle\tau\rangle_{min}}^{\langle\tau\rangle_{max}} R^{cc}(\tau)\langle f_{cas}(\tau)\rangle d\tau. \quad (9)$$

The calculations are performed with the input parameters varied in a wide range: $\beta = 4/3$ or $5/3$ (see [31]); cloud amount $N = 0.1$, 0.3, or 0.5; cloud geometric thickness $H = 0.5$ or 1 km; mean cloud optical thickness $\bar{\tau} = 6$, 13, or 26; and cloud single scattering albedo $\omega = 0.95$, 0.99, or 1.00. For most of the events, the parameter p is taken to be 0.35. The solar zenith angle varied in the range $0° \le \theta_0 \le 75°$.

The differences between the radiative characteristics obtained for each of the above models and for the cascade model (which is regarded as the reference model) are characterized by the relative error

$$\delta_{mod}(R) = 100\%(\langle R\rangle - \langle R\rangle_{mod})/\langle R\rangle, \quad R = S, A, Q_s, \quad (10)$$

where the subscript mod corresponds to the IPA, Poisson model, or HH model.

3.1. Independent Pixel Approximation, Cascade Model, and Horizontally Homogeneous Model

In the range of the aforementioned input parameters, the relations between the albedo values for the IPA, cascade model, and HH model depend on the solar zenith angle. For $0° \le \theta_0 \le 30°$, the inequality

$$A_{HH} > A_{IPA} \ge \langle A\rangle \quad (10a)$$

is fulfilled and the relative difference $\delta_{HH}(A)$ is about –25% (Fig. 7a). As the solar zenith angle increases further, the sign in the inequality between $\langle A\rangle$ and A_{IPA} changes at $\theta_0 = 60°$ and the difference between them increases:

$$A_{HH} > \langle A\rangle > A_{IPA}. \quad (10b)$$

At $\theta_0 = 75°$, the maximum mean albedo is obtained for the cascade model:

$$\langle A\rangle > A_{HH} > A_{IPA}. \quad (10c)$$

At $N = 0.5$, $\delta_{IPA}(A)$ is about 15% for $\theta_0 = 75°$. Note that these estimates are obtained for $\bar{\tau} = 13$; a decrease in the cloud optical thickness can reduce 3D effects (see also [21]).

In the case of conservative scattering, the relations for the transmission $T = 1 - A = Q_s + S$ follow from inequality (10). Let us consider the degree of agreement between the nonscattered and diffuse components of the downward radiation in these models.

The nonscattered fluxes in the IPA and HH model have a weak sensitivity to variations in the solar zenith angle, unlike those in the cascade model (Fig. 7b). The difference between $\langle S\rangle$ and S_{IPA} (and S_{HH}, having a similar value) increases with θ_0, and $\delta_{IPA}(S)$ is about –65% at $\theta_0 = 75°$. The diffuse transmission $Q_{s,\,IPA}$ depends more strongly on the solar zenith angle in comparison with $\langle Q_s\rangle$ and, at $\theta_0 = 75°$, $\delta_{IPA}(Q_s)$ reaches 45–55%, increasing as N and ω decrease (Fig. 7c). The HH cloud model leads to an even lower accuracy of the calculated Q_s values.

These differences are so significant because the IPA and the HH model are based on the solution of a one-dimensional deterministic RTE and, unlike the cascade model, do not take into account 3D effects of clouds. The causes determining the relations between $\langle A\rangle$ and A_{IPA} are detailed in [49]. At high solar zenith angles, the photons entering a cloud layer through its side boundaries (the cascade model) make an additional contribution to the transmission as compared to the photons

entering there through the upper boundary: $\langle Q_s \rangle > Q_{s,\mathrm{IPA}}$ (Fig. 7c) and $A_{\mathrm{IPA}} \geq \langle A \rangle$. As the solar zenith angle increases, the portion of reflected radiation consisting of photons entering the cloud through its side boundaries increases, the sign of the inequality changes to the opposite: $A_{\mathrm{IPA}} \leq \langle A \rangle$. Note that $A_{\mathrm{HH}} > A_{\mathrm{IPA}}$ always because the function $A(\tau)$ is convex.

The influence of the 3D-effects on the solar radiative transfer through broken clouds was discussed earlier in a number of works (see, e.g., [18, 21, 26]).

3.2. Cascade and Poisson Models

An analysis of the calculated results shows that the relative difference between the mean diffuse fluxes obtained on the basis of the cascade and Poisson models is no greater than 1–3% in most cases. It is important that, at fixed $\bar{\tau}$, σ_τ, N, H, and θ_0, the parameter γ chosen on the basis of relation (5) can be used in calculating $\rangle A \langle_{\mathrm{pois}}$ and $\rangle Q_s \langle_{\mathrm{pois}}$ not only in the case of conservative scattering but also in the presence of a moderate absorption of radiation by cloud drops ($\omega \geq 0.95$) (Fig. 7). At small solar zenith angles ($\theta_0 = 30°$), as the cloud amount decreases to $N = 0.1$, the mean cloud albedo decreases in both models and the error $\delta_{\mathrm{pois}}(A)$ may increase to about 5–7%. As the solar zenith angle θ_0 and $\bar{\tau}$ increase to 75° and 26, respectively, the $\delta_{\mathrm{pois}}(Q_s)$ value increases and can reach 10–20% depending on ω.

The mean radiative characteristics calculated on the basis of the Poisson model are in significantly better agreement with the results of the cascade model than the results of calculations in the IPA and HH approximation. This finding can be explained by the use of the CEM, which allows an accurate consideration for the effects caused by the random geometry of clouds (for details, see [6]).

The efficiency of the algorithm for mean-flux calculations in the Poisson model is significantly higher than in the cascade model. For example, at $\bar{\tau} = 13$ and $\theta_0 = 60°$, the ratio of computer times necessary for $\langle R \rangle$ and $\rangle R \langle_{\mathrm{pois}}$ calculations with the same relative error is greater than 100.

The computational burden for the cascade model is caused mainly by the necessity of simulation of cloud realizations and by the use of the maximum cross-section method for simulation of photon trajectories [37].

3.3. Dependence of the Parameter γ on the Solar Zenith Angle

In Section 3.2., the effective value of γ was obtained by us for each specific set of parameters N, H, θ_0, $\bar{\tau}$, and σ_τ. Let the parameters of the cloud field be insignificantly varied in a time interval within which variations in the solar zenith angle $\theta_0^{\min} \leq \theta_0(t) \leq \theta_0^{\max}$ can be substantial. In view of the stable state of clouds, it is logical to expect that, at constant N, H, $\bar{\tau}$, and σ_τ, there is a range of γ variations such that any value from the interval $\gamma_{\min} \leq \gamma \leq \gamma_{\max}$ can be used to calculate the diffuse radiation with a reasonable accuracy at any solar zenith angle ($\theta_0^{\min}$, $\theta_0^{\max}$). To test this assumption, we use the following approach.

Let us fix the values of N, H, $\bar{\tau}$, and σ_τ and calculate the Poisson model parameter $\gamma(\theta_0)$ from (5) for the range of zenith angles $30° \leq \theta_0 \leq 75°$. The range of $\gamma(\theta_0)$ variability depends on the input parameters: for example, at $\bar{\tau} = 13$, $\sigma_\tau = 12.1$, and $H = 1$ km, it is within the limits $0.32 \leq \gamma(\theta_0) \leq 0.41$ (2.45 km $\leq D \leq$ 3.13 km) for $N = 0.5$ and $0.53 \leq \gamma(\theta_0) \leq 0.79$ (1.27 km $\leq D \leq$ 1.88 km) for $N = 0.1$.

Let the permissible variability of the mean nonscattered radiation be no more than Δ_S. (In the subsequent calculations, we will assume that the corresponding relative difference $\delta_S = 100\% \times \Delta_S / \rangle S \langle_{\mathrm{pois}}$ is equal to 5% for the entire set of parameters.) For each θ_0, we choose $\gamma_{\min}(\theta_0)$ and $\gamma_{\max}(\theta_0)$ such that

$$\begin{aligned} \rangle S(\gamma_{\min}(\theta_0),\theta_0) \langle_{\mathrm{pois}} &= \rangle S(\gamma(\theta_0),\theta_0) \langle_{\mathrm{pois}} + \Delta_S(\theta_0), \\ \rangle S(\gamma_{\max}(\theta_0),\theta_0) \langle_{\mathrm{pois}} &= \rangle S(\gamma(\theta_0),\theta_0) \langle_{\mathrm{pois}} - \Delta_S(\theta_0). \end{aligned} \quad (11)$$

Figure 8a presents the functions $\gamma_{\min}(\theta_0)$ and $\gamma_{\max}(\theta_0)$ for the solar zenith angles $30° < \theta_0 \leq 75°$. It is evident that there is an interval of γ values $\gamma_{\min} \leq \gamma \leq \gamma_{\max}$ appropriate for all angles θ_0 under consideration. (The corresponding region is shaded in the figure.) This region corresponds to the interval of $\gamma(\theta_0)$ variation for the maximum solar zenith angle $\theta_0 = 75°$. For the input parameters indicated in the caption of Fig. 8, this interval is $0.29 \leq \gamma \leq 0.35$ (2.83 km $\leq D \leq$ 3.48 km). According to the Poisson model, the mean nonscattered fluxes depend only slightly on θ_0 near the zenith . Therefore, it is believed that the interval ($\gamma_{\min}$, $\gamma_{\max}$) can be extended to a wider range of variation $0° \leq \theta_0 \leq 75°$. It is necessary to take into account that the interval ($\gamma_{\min}$, $\gamma_{\max}$) depends on the cloud amount and on the statistical characteristics of τ.

Let us calculate the mean radiation fluxes by the Poisson model of broken clouds, $\rangle R(\gamma_{\min}) \langle_{\mathrm{pois}}$ and $\rangle R(\gamma_{\max}) \langle_{\mathrm{pois}}$, where $R = S$, A, or Q_s. An analysis of these results shows that the relative difference between the mean nonscattered fluxes $\langle S \rangle$ and $\rangle S(\gamma) \langle_{\mathrm{pois}}$ and albedo $\langle A \rangle$ and $\rangle A(\gamma) \langle_{\mathrm{pois}}$ does not exceed 5% and the relative difference between the corresponding diffuse transmissions does not exceed 10% at any angles $0° \leq \theta_0 \leq 75°$ for $\gamma_{\min} \leq \gamma \leq \gamma_{\max}$. This difference can increase somewhat when the mean diffuse fluxes decrease. For example, as N decreases, the albedo differences increase to 10% and, as $\bar{\tau}$ increases and ω decreases, the diffuse-transmission differences can increase to 20%. However, in this case as well, the mean radiative characteristics

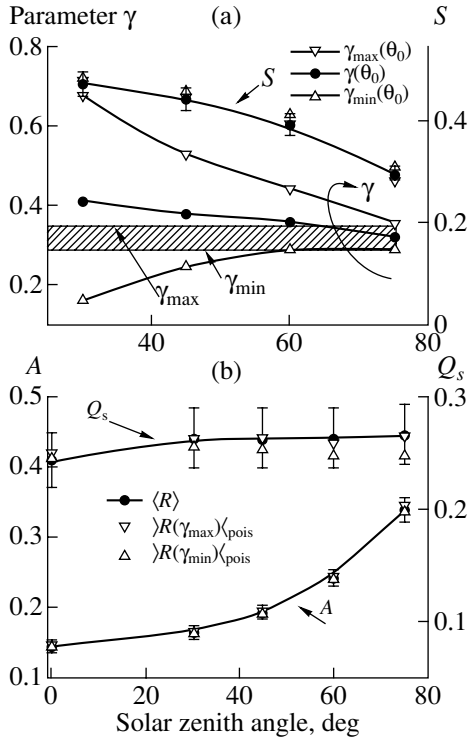

Fig. 8. (a) Range of parameter γ corresponding to Eq. (11); the range $\gamma_{min} \le \gamma \le \gamma_{max}$ applicable to Eq. (11) at $0° \le \theta_0 \le 75°$ is dashed. (a, b) Mean fluxes in the cascade and Poisson models are calculated for γ_{min} and γ_{max} at $\omega = 0.99$ and at all other parameters as in Fig. 7. In the cascade model, variations in the mean fluxes are 5% for S and A and 10 % for Q_s.

obtained in the Poisson model are in better agreement with the cascade model than those obtained in the IPA and in the HH models.

Thus, the effective γ values chosen in the interval $\gamma_{min} \le \gamma \le \gamma_{max}$ provide a reasonable accuracy of calculated diffuse fluxes for a wide range of solar zenith angles. This result testifies that the approach used by us for calculation of the effective γ values characterizes the geometric structure of cloud fields correctly on the whole.

CONCLUSIONS

This study concerns the problem of validation of the statistically homogeneous Poisson model of clouds and represents the continuation of the studies started in [6]. As the prototype of subgrid-scale real cloud fields, we used realizations of the fractionally integrated cascade model of broken clouds. A comparative analysis was performed on the basis of a new approach to the choice of input parameters for the Poisson model. This approach includes

(1) consideration for variations in the cloud optical thickness by averaging in accordance with the probability density $\langle f_{cas}(\tau)\rangle$ and

(2) fitting of the effective γ value such that the cascade and Poisson models lead to identical fluxes of nonscattered radiation. (The following conditions should also be fulfilled: $N < 0.7$ and $\theta_0 \ge 30°$.)

The results of numerical simulation have shown that our approach provides an agreement within 1–3% of the mean diffuse fluxes in a wide range of input parameters. The disagreement increases somewhat as the mean fluxes decrease; in particular, an increase in $\bar{\tau}$ leads to an increase in $\delta_{pois}(Q_s)$ to 10–20% depending on ω. It is important that the same γ values can be used for calculations in the case of conservative scattering and in the presence of moderate absorption by liquid drops ($\omega \ge 0.95$). Moreover, if the optical characteristics and the geometric cloud thickness are fixed, there is a range $\gamma_{min} \le \gamma \le \gamma_{max}$ such that, in most cases, the error of mean-flux calculations is no greater than 5 to 10% for all solar zenith angles $0° \le \theta_0 \le 75°$.

Thus, the Poisson cloud model shows promise for use in calculations of radiative characteristics of subgrid-scale cloud fields owing to its following advantages:

(1) The computational burden is two or more orders of magnitude lower than that characteristic of the cascade model.

(2) The calculations of area-averaged radiation fluxes are more accurate than those provided by the IPA and the HH cloud models because the Poisson cloud model allows consideration for the effects caused by the random geometry of clouds.

The results obtained by us can be useful for comparison of area-averaged scattered fluxes with the data of field measurements: when measured data on the structure of real cloud fields are deficient, the effective value of γ can be calculated from measurements of nonscattered radiation. The problem of how much would this value be in agreement with the physical value $\gamma = H/D$ is the subject of further investigations. Its solution is related to the accumulation and use of the data of satellite and ground-based measurements carried out, in particular, at the sites of the Atmospheric Radiation Measurement (ARM) Program.

ACKNOWLEDGMENTS

This work was supported in part by the DOE's ARM Program, project no. DE-A-105-90ER61069 and contract no. 5012; by the Russian Foundation for Basic Research, project no. 03-05-64655a; and INTAS project no. 01-0239.

APPENDIX

As is shown in [31, 50, 51], the liquid water distribution in marine stratocumulus clouds (*Sc*) is characterized by the power-law spectral density $E(k) \propto k^{-\beta}$ ($k = \pi/r$ is the wave number and r is the scale, km) for spatial

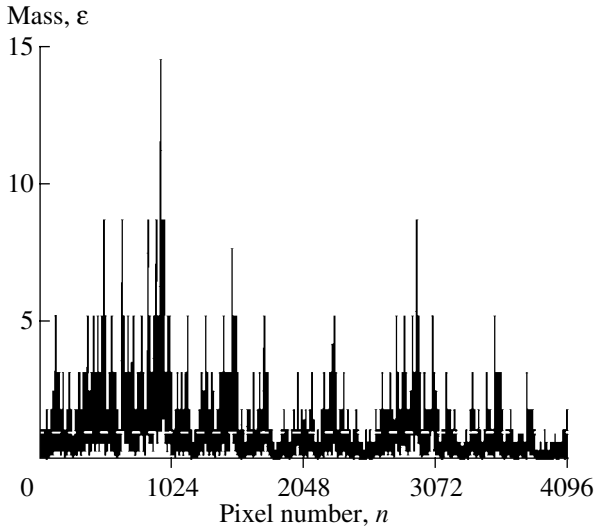

Fig. 9. Multiplicative cascade p-model: $p = 0.375$, $\beta_\varepsilon = 0.91$, $\bar{\varepsilon} = 1$, and the number of pixels $N_{\text{pix}} = 2^{12}$.

scales varying within at least three orders of magnitude. This implies that stochastic models used for simulation of LWP fluctuations are bound to be spatially invariant.

Below, the simplest one-dimensional case is considered to show how a multiplicative cascade model satisfying the condition of spatial invariance is constructed [13, 31]. Let us consider a plane-parallel homogeneous layer of finite length L. We divide this layer into two segments, and a liquid-water portion f_1 is transported from one segment to the other in a random direction. This operation is analogous to the multiplication of the initially specified uniform probability density of the LWP by $W_1^{(\pm)} = 1 \pm f_1$. At the next step, we divide each of these segments into two and transport a liquid-water portion f_2 from one quarter of the cloud layer to the neighboring one in a direction chosen randomly and independently. Then, we repeat such a procedure with a smaller segment of the smaller size r_{i+1}, where $r_{i+1} = L/2^i$. This segment contains a liquid-water portion f_i ($i = 3, 4, \ldots$). As a result, the initial plane-parallel layer will be divided into pixels uniform in size but with different LWPs.

Singular Cascades

We parameterize the multiplicative weights:

$$W_i^{(\pm)} = 1 \pm f_i = 1 \pm (1-2p) = \begin{Bmatrix} 2p \\ 2(1-p) \end{Bmatrix}, \quad 0 \le p \le \frac{1}{2}, \quad i = 1, 2, \ldots. \tag{A.1}$$

At any i, the probability that the sign of the f_i increment is positive or negative is 50%. Such a parametrization leads to a singular multifractal model, which is termed a p-model [52]: the parameter p controls the mass (energy) ε redistributed at each step. The p-model (Fig. 9) is spatially invariant and has the wave-number spectrum

$$E_\varepsilon(k) \approx k^{-\beta_\varepsilon}, \quad k > 0,$$

where the exponent is determined by the relation

$$0 \le \beta_\varepsilon(p) = 1 - \log_2[1 + (1-2p)^2] < 1.$$

For real cloud fields, the exponent $\beta > 1$. Therefore, to simulate LWP fluctuations within continuous cloud layers, the problem of p-model transformation should be solved.

Limited Cascades

The easiest way to obtain $\beta > 1$ lies in reducing variations in multiplicative weights (A.1) at each step. Choosing

$$W_i^{(\pm)} = 1 \pm (1-2p)^{-\alpha i}, \quad 0 \le p < \frac{1}{2}, \quad \alpha > 0, \quad i = 1, 2, \ldots,$$

we obtain "limited" cascade models [13]. The point $\alpha = 0$ is singular and corresponds to a singular model. The variability range for the exponent β corresponding to the new field φ transforms into the interval

$$1 < \beta_\varphi(\alpha) = \min\{2\alpha, 1\} + 1 \le 2$$

independently of p. Figure 10a presents the realization corresponding to 14 steps of the limited cascade φ-model with $\alpha = 1/3$ and $p = 0.375$.

Fractional Integration

Another way of transforming singular cascades with $\beta_\varepsilon < 1$ into more realistic cascades with $\beta_\varphi > 1$ lies in filtering in the Fourier space [25]

$$\varphi(x) = \int \varepsilon(y)|x-y|^{\alpha^* - 1} dy. \tag{A.2}$$

This operation, also known as the fractional integration, involves convolution with a weakly singular kernel. Varying the α^* value, we can switch from the field with $\beta_\varepsilon < 1$ to the field in which β_φ is equal to the preset value

$$\beta_\varphi(p, \alpha^*) = \beta_\varepsilon(p) + 2\alpha^*. \tag{A.3}$$

An example of realization of the fractionally integrated cascade φ-model is presented in Fig. 10b for $p = 0.375$ ($\beta_\varepsilon(p) = 0.91$) and $\alpha^* = 0.38$ ($\beta_\varphi(p, \alpha^*) = 5/3$). The model obtained on the basis of relation (A.2a) is referred to as the fractionally integrated cascade model. It can be used for description of the liquid water distribution in continuous cloud layers.

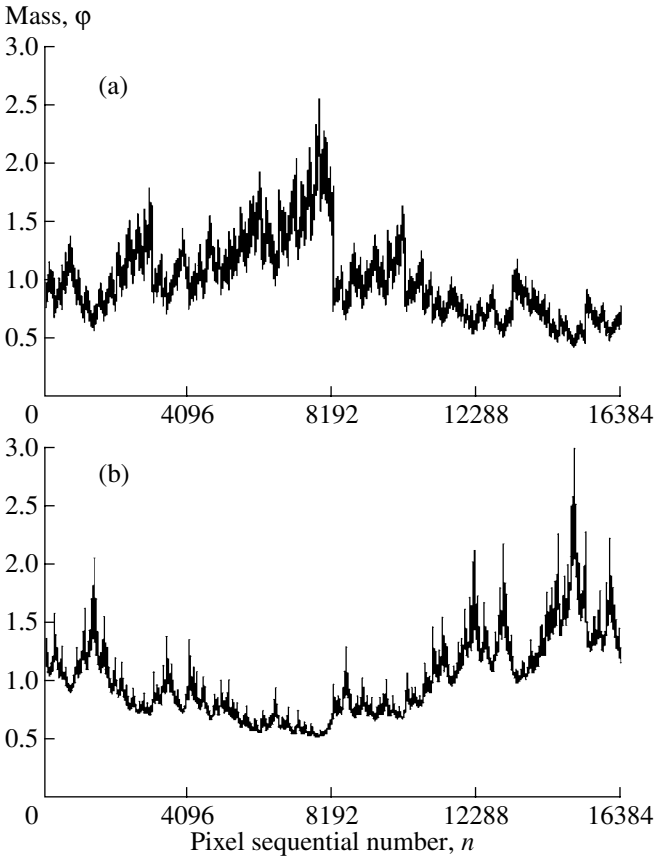

Fig. 10. Fractal models with the same β, p, and $\bar{\varphi}$ values equal to 5/3, 3/8, and 1, respectively: (a) bounded cascades, $\alpha = 1/3$, and (b) the fractionally integrated model, $\alpha^* = 0.38$. The number of pixels $N_{pix} = 2^{14}$.

Switching from a one-dimensional case to a two-dimensional cascade model is detailed in [53].

REFERENCES

1. Harshvardhan and D. Randall, "Comments on 'the Parameterization of Radiation for Numerical Weather Prediction and Climate Models,'" Mon. Weather Rev. **113**, 1832–1833 (1985).
2. G. L. Stephens, "Reply (to Harshvardhan and Randall)," Mon. Weather Rev. **113**, 1834–1835 (1985).
3. G. L. Stephens and C. M. Platt, "Aircraft Observations of the Radiative and Microphysical Properties of Stratocumulus and Cumulus Cloud Fields," J. Clim. Appl. Meteorol. **26**, 1243–1269 (1987).
4. Yu.-A. Mullamaa, M. A. Sulev, V. K. Pyldmaa, *et al.*, *Stochastic Structure of the Fields of Clouds and Radiation* (Institut Fiziki i Astronomii, Akad. Nauk ESSR, Tartu, 1972) [in Russian].
5. B. A. Kargin, *Statistical Simulation of the Field of Solar Radiation in the Atmosphere* (VTs SO AN SSSR, Novosibirsk, 1984) [in Russian].
6. V. E. Zuev and G. A. Titov, *Atmospheric Optics and Climate* (IOA SO RAN, Tomsk, 1996) [in Russian].
7. H. W. Barker and J. A. Davies, "Cumulus Cloud Radiative Properties and the Characteristics of Satellite Radiance Wavenumber Spectra," Remote Sensing Environ. **42**, 51–64 (1992).
8. F. Malvagi, R. N. Byrne, G. Pomraning, and R. C. J. Somerville, "Stochastic Radiative Transfer in a Partially Cloudy Atmosphere," J. Atmos. Sci. **50**, 2146–2158 (1993).
9. S. M. Prigarin and G. A. Titov, "Spectral Methods of Numerical Simulation of Geophysical Fields," Opt. Atmos. Okeana **9**, 993–1003 (1996).
10. I. V. Geogdzhaev, T. V. Kondranin, A. N. Rublev, and N. E. Chubarova, "UV Radiation Transfer through Broken Cloud Fields: Modeling and Comparison with Measurements," Izv. Akad. Nauk, Fiz. Atmos. Okeana **33**, 680–686 (1997) [Izv., Atmos. Ocean. Phys. **33**, 630–635 (1997)].
11. K. F. Evans, S. McFarlane, and W. J. Wiscombe, "Three-Dimensional Radiative Transfer Effects of Two-Point Statistical Representations of Broken Cloud Structure," in *Proceedings of 10th AMS Conference on Atmospheric Radiation, Madison, WI, 1999* (American Meteorological Society, Boston, 1999), pp. 579–582.
12. R. F. Cahalan, W. Ridgway, W. J. Wiscombe, *et al.*, "Independent Pixel and Monte Carlo Estimates of Stratocumulus Albedo," J. Atmos. Sci. **51**, 3776–3790 (1994).
13. R. F. Cahalan, W. Ridgway, W. J. Wiscombe, *et al.*, "The Albedo of Fractal Stratocumulus Clouds," J. Atmos. Sci. **51**, 2434–2455 (1994).
14. H. Barker, "A Parameterization for Computing Grid-Averaged Solar Fluxes for Inhomogeneous Marine Boundary Layer Clouds. Part I: Methodology and Homogeneous Biases," J. Atmos. Sci. **53**, 2289–2303 (1996).
15. L. Oreopoulos and H. W. Barker, "Accounting for Subgrid-Scale Cloud Variability in a Multilayer 1D Solar Radiative Transfer Algorithm," Q.J.R. Meteorol. Soc. **125** (553), 301–330 (1999).
16. H. Barker, B. Wielicki, and L. Parker, "A Parameterization for Computing Grid-Averaged Solar Fluxes for Inhomogeneous Marine Boundary Layer Clouds. Part II: Validation Using Satellite Data," J. Atmos. Sci. **53**, 2304–2316 (1996).
17. L. H. Chambers, B. Wielicki, and K. F. Evans, "Independent Pixel and Two-Dimensional Estimates of Landsat-Derived Cloud Field Albedo," J. Atmos. Sci. **54**, 1525–1532 (1997).
18. P. Zuidema and K. F. Evans, "On the Validity of the Independent Pixel Approximation for Boundary Layer Clouds Observed During ASTEX," J. Geophys. Res. D **103**, 6059–6074 (1998).
19. W. O'Hirok and C. Cauttier, "A Three-Dimensional Radiative Transfer Model to Investigate the Solar Radiation with a Cloudy Atmosphere. Part I: Spatial Effects," J. Atmos. Sci. **55**, 2162–2179 (1998).
20. H. W. Barker, J. J. Morcrette, and G. D. Alexander, "Broadband Solar Fluxes and Heating Rates for Atmospheres with 3D Broken Clouds," Q. J. R. Meteorol. Soc. **124** (548), 1245–1271 (1998).
21. T. C. Benner and K. F. Evans, "Three Dimensional Solar Radiative Transfer in Small Tropical Cumulus Fields

Derived from High-Resolution Imagery," J. Geophys. Res. D **106**, 14975–14984 (2001).

22. G. W. Petty, "Area-Average Solar Radiative Transfer in Three-Dimensionally Inhomogeneous Clouds: The Independently Scattering Cloudlet Model," J. Atmos. Sci. **59**, 2910–2929 (2002).
23. E. Kassianov, T. P. Ackerman, R. Marchand, and M. Ovtchinnikov, "Stochastic Radiative Transfer in Multilayer Broken Clouds. Part II: Validation Test," J. Quant. Spectrosc. Radiat. Transfer **77**, 395–416 (2003).
24. D. Lane, E. K. Goris, and R. C. J. Somerville, "Radiative Transfer through Broken Clouds: Observations and Model Validation," J. Clim. **15**, 2921–2933 (2002).
25. D. Schertzer and S. Lovejoy, "Physical Modeling and Analysis of Rain and Clouds by Anisotropic Scaling Multiplicative Processes," J. Geophys. Res. D **92**, 9693–9714 (1987).
26. A. Marshak, A. Davis, W. J. Wiscombe, *et al.*, "Biases in Shortwave Column Absorption in the Presence of Fractal Clouds," J. Clim. **11**, 431–446 (1998).
27. E. Kassianov, "Stochastic Radiative Transfer in Multilayer Broken Clouds. Part I: Markovian Approach," J. Quant. Spectrosc. Radiat. Transfer **77**, 373–394 (2003).
28. S. Lovejoy, A. Davis, P. Gabriel, *et al.*, "Discrete Angle Radiative Transfer I: Scaling and Similarity, Universality and Diffusion," J. Geophys. Res. D **95**, 11699–11715 (1990).
29. R. Cahalan and J. Snider, "Marine Stratocumulus Structure," Remote Sensing Environ. **28**, 95–107 (1989).
30. R. Cahalan and J. Joseph, "Fractal Statistics of Cloud Fields," Mon. Weather Rev. **117**, 261–272 (1989).
31. A. Davis, A. Marshak, W. Wiscombe, and R. Cahalan, "Scale-Invariance in Liquid Water Distributions in Marine Stratocumulus. Part I: Spectral Properties and Stationarity Issues," J. Atmos. Sci. **53**, 1538–1558 (1996).
32. B. B. Mandelbrot, *Fractals: Form, Chance, and Dimension* (Freeman, San Francisco, 1977).
33. R. F. Cahalan, "Bounded Cascade Clouds: Albedo and Effective Thickness," Nonlinear Processes Geophys. **1** (2/3), 156–167 (1994).
34. B. Wielicki and L. Parker, "Frequency Distributions of Cloud Liquid Water Path in Oceanic Boundary Layer Cloud As a Function of Regional Cloud Fraction," in *Preprint of 8th Conference on Atmospheric Radiation 1994* (American Meteorological Society, Nashville, TN, 1994), pp. 415–418.
35. G. A. Mikhailov, *Optimization of Monte Carlo Weight Methods* (Nauka, Moscow, 1987) [in Russian].
36. G. A. Mikhailov, "On the Randomization of the Algorithms of the Monte-Carlo Method," in *Statistical Simulation in Mathematical Physics* (VTs SO RAN SSSR, Novosibirsk, 1976), pp. 5–16 [in Russian].
37. G. I. Marchuk, G. A. Mikhailov, M. A. Nazaraliev, *et al.*, *Monte Carlo Method in Atmospheric Optics* (Nauka, Novosibirsk, 1976) [in Russian].
38. D. Deirmendjian, *Electromagnetic Scattering on Spherical Polydispersions* (Elsevier, New York, 1969; Mir, Moscow, 1971).
39. *Clouds and Cloudy Atmosphere. Handbook*, Ed. by I. P. Mazin and A. Kh. Khrgian (Gidrometeoizdat, Leningrad, 1989) [in Russian].
40. T. B. Zhuravleva and A. L. Marshak, "Validation of the Poisson Stochastic Radiative Transfer Model against Cloud Cascade Models," http://www.arm.gov/dos/documents/technical/conf_0304/zhuravleva-tb.pdf.
41. R. F. Cahalan, M. McGill, J. Kolasinski, *et al.*, "THOR—Cloud Thickness from Offbeam Lidar Returns," J. Atmos. Ocean Techn. **22**, 605–627 (2005).
42. B. C. Benner and J. A. Curry, "Characteristics of Small Tropical Cumulus Clouds and Their Impact on the Environment," J. Geophys. Res. D **103**, 28753–28767 (1998).
43. K. Hozumi, T. Harymaya, and C. Magono, "The Size Distribution of Cumulus Clouds As a Function of Cloud Amount," J. Meteorol. Soc. Jpn. **60**, 691–699 (1982).
44. B. A. Wielicki and R. M. Welch, "Cumulus Cloud Properties Derived Using Landsat Satellite Data," J. Appl. Meteorol. **25**, 251–276 (1986).
45. V. G. Plank, "The Size Distribution of Cumulus Clouds in Representative Florida Populations," J. Appl. Meteorol. **8**, 46–67 (1969).
46. R. M. Welch, K. S. Kuo, B. A. Weilicki, *et al.*, "Marine Stratocumulus Cloud Fields of the Coast of Southern California Observed Using LANDSAT Imagery. Part I: Structural Characteristics," J. Appl. Meteorol. **27**, 341–361 (1988).
47. S. Platnick, M. D. King, S. A. Ackerman, *et al.*, "The MODIS Cloud Products: Algorithms and Examples from Terra," IEEE Trans. Geosci. Remote Sensing **41**, 459–473 (2003).
48. G. L. Stephens, D. Vane, R. Boain, *et al.*, "The CloudSat Mission and the A-Train: A New Dimension of Space-Based Observations of Clouds and Precipitation," Bull. Am. Meteorol. Soc. **83**, 1771–1790 (2002).
49. A. Davis and A. Marshak, "Multiple Scattering in Clouds: Insights from Three-Dimensional Diffusion Theory," Nuclear Sci. Eng. **137**, 251–280 (2001).
50. Y. Tessier, S. Lovejoy, and D. Schertzer, "Universal Multifractals: Theory and Observations for Rain and Clouds," J. Appl. Meteorol. **32**, 223–250 (1993).
51. A. Marshak, A. Davis, W. Wiscombe, and R. Cahalan, "Scale Invariance of Liquid Water Distributions in Marine Stratocumulus. Part 2: Multifractal Properties and Intermittency Issues," J. Atmos. Sci. **54**, 1423–1444 (1997).
52. C. Meneveau and K. R. Screenivasan, "Simple Multifractal Cascade Model for Fully Developed Turbulence," Phys. Rev. Lett. **59**, 1424–1427 (1987).
53. A. Marshak, A. Davis, W. Wiscombe, and G. Titov, "The Verisimilitude of the Independent Pixel Approximation Used in Cloud Remote Sensing," Remote Sensing Environ. **52**, 71–78 (1995).

Translated by E. Kadyshevich